ACS APPLIED MATERIALS & INTERFACES

Research Article

www.acsami.org

Preparation and Fuel Cell Performance of Catalyst Layers Using Sulfonated Polyimide Ionomers

Takuya Omata,[†] Manabu Tanaka,[‡] Kenji Miyatake,*[,‡,§] Makoto Uchida,[‡] Hiroyuki Uchida,[‡,§] and Masahiro Watanabe*[,‡]

[†]Interdisciplinary Graduate School of Medicine and Engineering, [‡]Fuel Cell Nanomaterials Center, [§]Clean Energy Research Center, University of Yamanashi, 4 Takeda, Kofu 400-8510, Japan

Supporting Information

ABSTRACT: Sulfonated polyimide (SPI-8) ionomers were used as binders in the catalyst layers, and their fuel cell performance was evaluated. SPI-8 ionomers functioned well in the anode with only minor overpotential even at low humidity (50% relative humidity (RH)). In contrast, the cathode performance was significantly dependent on the content and molecular weight of the ionomers and humidity of the supplied gases. Higher molecular weight of the ionomer caused larger potential drop at high current density at 80 and 100% RH since oxygen supply and/or water discharge became insufficient due to higher water uptake (swelling) of the ionomer. Similar results were obtained at higher ionomer content, because of the increase of thickness in the catalyst layer. The mass transport was improved with decreasing humidity, however, proton conductivity became lower. While the maximum values of $j_{@0.70\ V}$ for all membrane electrode assemblies (MEAs) were ca. 0.35 A/cm^2, each electrode could have the different appropriate operating conditions. The results suggest that the parameters such as oxygen supply, proton conductivity, and water uptake and discharge need to be carefully optimized in the catalyst layers for achieving reasonable cathode performance with hydrocarbon ionomers.

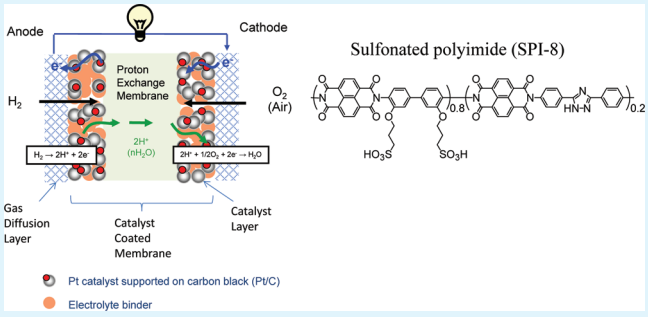

KEYWORDS: *fuel cells, catalyst layers, hydrocarbon ionomers, sulfonated polyimides*

INTRODUCTION

Polymer electrolyte fuel cells (PEFCs) have attracted considerable attention as alternative power sources for stationary, portable, and transportation applications due to their high efficiency and low pollutant emissions. For the practical commercialization of PEFCs, performance, durability, and cost need to be improved. Much effort has been devoted for the development of highly active electrocatalysts and highly proton conductive polymers. As proton conductive polymers, perfluorinated sulfonic acid (PFSA) ionomers such as Nafion are state-of-the-art and most used. They are highly proton conductive and durable under fuel cell operating conditions. However, there has been a great demand for alternative ionomers based on nonfluorinated hydrocarbon materials from the viewpoint of high temperature availability, environmental compatibility, and low production cost.

A number of hydrocarbon ionomers have been developed in the past decade. Most research focuses on the synthesis and properties of hydrocarbon ionomer membranes.[1−11] There have been few reports on the properties of such emerging ionomer materials as a binder in the catalyst layer of the gas diffusion electrodes.[12−22] In the literature, there was a report on sulfonated poly(ether ether ketone) (SPEEK) as a binder. Effect of the content and ion exchange capacity (IEC) of the binder on the fuel cell performance was investigated;[16,17] however, the performance was inferior compared with that of the gas diffusion electrodes with Nafion binder. We reported preparation and fuel cell performance of gas diffusion electrodes using our sulfonated poly(arylene ether)s (SPEs) as a cathode binder.[21,22] In addition to the content and IEC of the binder, operating humidity was another crucial factor in determining fuel cell performance since properties (water absorbability, proton conductivity, and specific adsorbability on electrocatalysts) of aromatic ionomers depend severely on water activity.

Recently, we have synthesized novel sulfonated polyimide ionomers containing triazole groups (sulfonated polyimide (SPI-8)).[8] The SPI-8 membrane with high IEC of 2.4 mequiv·g^{-1} exhibited comparable proton conductivity to that of Nafion at high temperature. The SPI-8 membrane was durable in operating fuel cells for 5000 h at 80 °C and constant current density of 0.2 A/cm^2.[23] The fuel cell utilized Nafion as a binder in the catalyst layer. The objective of this study is to evaluate SPI-8 ionomers as a binder in the catalyst layer for both electrodes. Catalyst-coated-membranes (CCMs) with the catalyst layers containing the SPI-8 as a binder were prepared,

Received: October 4, 2011
Accepted: December 27, 2011
Published: December 27, 2011

in which Nafion was used as the membrane. The fuel cell performance of the CCMs was investigated in detail at various humidities to optimize the content and molecular weight of the SPI-8 binder.

EXPERIMENTAL SECTION

Preparation of Catalyst Coated Membranes (CCMs). Sulfonated polyimide (SPI-8) ionomers were synthesized according to the previously reported method.[8] Three SPI-8s with different chain lengths (degree of polymerization: n = 5, 50, 285), denoted as SPI-8_5, SPI-8_{50}, and SPI-8_{285}, respectively, were synthesized by changing the comonomer feed ratio. Catalyst-coated-membranes (CCMs) were prepared by the decal method (Figure S1, Supporting Information). A catalyst ink was prepared by mixing Pt catalyst supported on carbon black (Pt/C, TEC10E70TPM, 67 wt %, Tanaka Kikinzoku Kogyo K.K.) with 3 (SPI-8_{285} and SPI-8_{50}) or 5 (SPI-8_5) wt % SPI-8 solution in dimethylsulfoxide (DMSO) using a planetary ball-mill for 30 min. The mass ratio of SPI-8 to carbon black (SPI-8/C) was set at 0.5, 0.7, or 1.0. The ink was uniformly coated on an aluminum foil using a screen printer (Newlong Seimitsu Kogyo Co., Ltd.) to form a catalyst layer. Lack of aluminum ion contamination was confirmed by ICP-mass spectra. The catalyst layer was dried at 80 °C under vacuum and cut into a circle (3.8 cm^2). A CCM was prepared by hot-pressing an Nafion NRE212 membrane (Dupont, 50 μm thick) between two catalyst layers at 140 °C and 1.0 MPa for 3 min. The aluminum foils were peeled off from the catalyst layers. The obtained CCM as membrane electrode assembly (MEA) was then combined with gas diffusion layers (GDLs, 25BCH, SGL Carbon Group Co., Ltd.) and mounted into an in-house designed circular test cell consisting of two carbon separator plates and a reversible hydrogen electrode (RHE).

Fuel Cell Operation. The cell was operated at 80 °C supplying H_2 to the anode and air to the cathode at ambient pressure. The gas flow rate was controlled at 200 mL/min by a mass flow controller. The utilization of H_2 and air was 13.0% and 32.5% at the current density of 1 A/cm^2, respectively. The gases were humidified at 50, 60, 70, 80, or 100% RH (relative humidity). Current–potential (I–E) curves and ohmic potential (IR) drops were measured with a current interrupter (NCPG 1010, Nikko Keisoku) under steady-state operation. The IR drop was measured by applying current-off pulse for 100 μs to the cell, and the resulting potential drop was recorded with a storage oscilloscope (VC6023, Hitachi). Electrochemically active surface area (ECA) of Pt at the cathode catalyst layer was estimated by cyclic voltammetry (CV) at 40 °C using a potentiostat (PGST30 Autolab system, Eco-Chemie). During the CV measurement, H_2 gas (100 mL/min, 100% RH) was supplied to the anode, and the cathode compartment was purged with N_2 (150 mL/min, 100% RH). Prior to the potential sweep, the potential was maintained at 0.085 V for 3 s to ensure the metallic (reduced) state of the Pt catalysts. Then, N_2 flow was stopped, and the potential was swept from 0.085 to 1.000 V at 20 mV/s. The ECA values were calculated from the hydrogen adsorption charge in the negative-going potential scan, referred to ΔQ_H^o = 0.21 mC/cm^2, adopted conventionally for clean polycrystalline platinum.[24,25] CV curves were also measured at 80 °C, 50–100% RH.

Scanning Transmission Electron Microscopic (STEM) Observations. The SPI-8 coated Pt/C catalyst was scratched from the catalyst layers and attached on the tip of needle of FIB/STEM compatible holder with a specially designed tilt mechanism.[26] Images were taken on a Hitachi HD-2700 STEM using an accelerating voltage of 80 kV.

RESULTS AND DISCUSSION

Effect of Molecular Weight of SPI-8 Ionomer on the Anode and the Cathode Performance. Figure 1 shows IR-free anode and cathode polarization curves obtained for MEAs with SPI-8 ionomer used as binder in both electrodes at 50, 80, and 100% RH. In order to evaluate the effect of molecular weight of the binder on the electrode performance, three SPI-8s with different molecular weights (SPI-8_5, SPI-8_{50}, and SPI-8_{285})

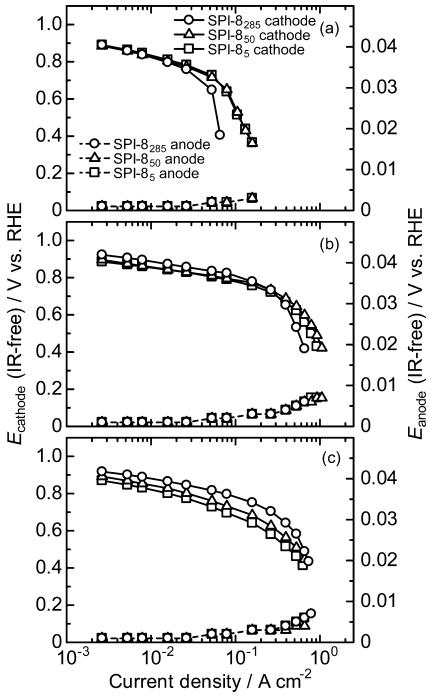

Figure 1. Steady-state anode and cathode polarization curves for MEAs with SPI-8_5 (square), SPI-8_{50} (triangle), and SPI-8_{285} (circle) binders at (a) 100% RH, (b) 80% RH, and (c) 50% RH at the cell temperature of 80 °C.

were used. The polarization curves were measured by feeding hydrogen as a fuel and air as an oxidant at 80 °C. The anode polarization was very similar for the three MEAs and negligibly small when the current density was lower than 0.1 A/cm^2. The anode polarization became slightly larger with a decrease in the humidity because of the decreased proton conductivity of SPI-8 at low humidity.[8] Increasing the current density also resulted in an increase of the anode polarization since electro-osmotic drag of water from the anode to the cathode could dry the anode catalyst layer.

Compared to the anode polarization, cathode polarization was much more significant. At 100% RH, cathode potential dropped at high current density. As reported in our previous work, the cathode polarization at high humidity could result from large swelling of hydrocarbon binder.[21] The excessive swelling causes (i) an increase of thickness of the binder covering on Pt/C catalysts, and (ii) a decrease of pore volume in the catalyst layer. Both of these disturb mass transport (e.g., oxygen supply and/or water discharge) in the cathode catalyst layers. The largest drop was observed for the MEA with SPI-8_{285}. Since high molecular weight SPI-8_{285} showed higher water uptake and more swelling compared to the low molecular weight SPI-8 (Figure S2, Supporting Information), the large potential drop for the MEA with SPI-8_{285} would result from the insufficient mass transport. The MEA with SPI-8_{285} showed better cathode performance at lower humidity because of the improved mass transport capability. At 50% RH, SPI-8_{285} MEA showed the highest cathode potential at wide range of current density. The results are reasonable since proton transport is more crucial than the swelling under low humidity conditions. The proton conductivity of higher molecular weight SPI-8_{285} is much higher than that of lower molecular weight SPI-8 at low humidity (Figure S2, Supporting Information).

dx.doi.org/10.1021/am201360j | ACS Appl. Mater. Interfaces 2012, 4, 730–737

The ohmic resistances of the cells are shown in Figure 2. At high humidity (80% and 100% RH), the ohmic resistances of

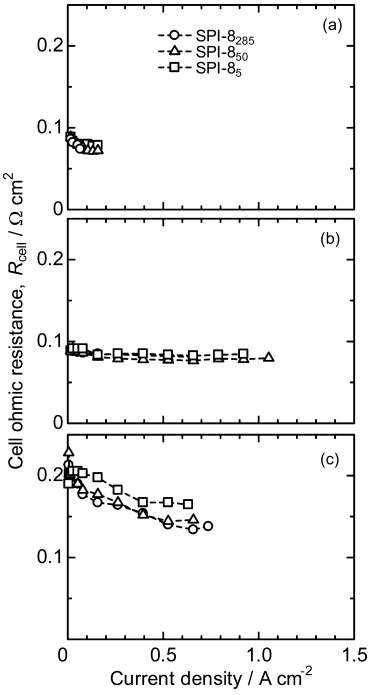

Figure 2. Ohmic resistances of the cells (R_{cell}) for MEAs with SPI-8_5 (square), SPI-8_{50} (triangle), and SPI-8_{285} (circle) binders at (a) 100% RH, (b) 80% RH, and (c) 50% RH at the cell temperature of 80 °C.

the three MEAs were somewhat higher than those expected from the proton conductivity and thickness of Nafion NRE 212 membrane (0.046 and 0.034 Ω cm^2 at 80% and 100% RH, respectively). The differences would be ascribed to the contact resistance between the SPI-8-containing electrodes and Nafion membrane. At 50% RH, the ohmic resistance of the MEA with SPI-8_5 was higher compared to those of the MEAs with SPI-8_{50} and SPI-8_{285}. The lower proton conductivity of SPI-8_5 at low humidity resulted in higher contact resistance. In addition, lower water absorbability of SPI-8_5 might have caused a smaller amount of water migration from the cathode to the membrane which accounts for higher Nafion membrane resistance.

Effect of SPI-8/Carbon Ratio on the Cathode Performance. Effect of SPI-8 content in the catalyst layers on the cathode performance was investigated (Figures 3 and 4). The cathode performance was significantly affected by the SPI-8 content. At 100% and 80% RH (Figure 3a,b), smaller content of SPI-8 resulted in better cathode performance. The results are not contradictory to the above-mentioned results, in which mass transport was crucial at high humidity. Provided that the volume of the catalyst layer was mainly occupied by carbon catalyst support (density = 2.0 g/cm^3) and SPI-8 binder (density = ca. 1.6 g/cm^3 at dry), the thickness of the catalyst layer at SPI-8/C = 0.5 was estimated to be 87% of that at SPI-8/C = 0.7 at the same Pt loading. It is reasonable to assume that the thinner cathode layer at lower binder content has better mass transport capability at high humidity. In addition, the porosity in the catalyst layer, which could be affected by the binder content, may also be responsible for the cell performance. The ohmic resistance of the cell was not affected by the SPI-8 content at 100% and 80% RH (Figure 4a,b), implying

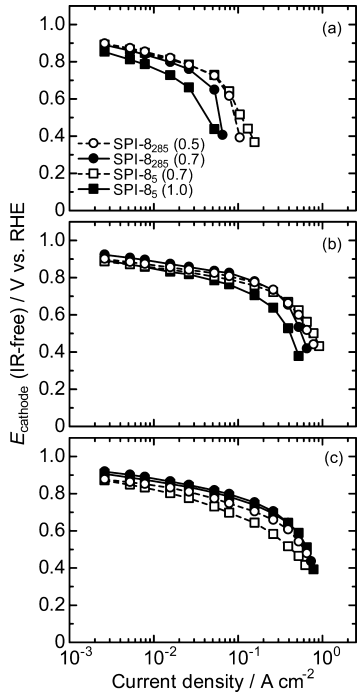

Figure 3. Steady-state cathode polarization curves for MEAs with SPI-8_{285} (0.5) (open circle), SPI-8_{285} (0.7) (closed circle), SPI-8_5 (0.7) (open square), and SPI-8_5 (1.0) (closed square) binders at (a) 100% RH, (b) 80% RH, and (c) 50% RH at the cell temperature of 80 °C.

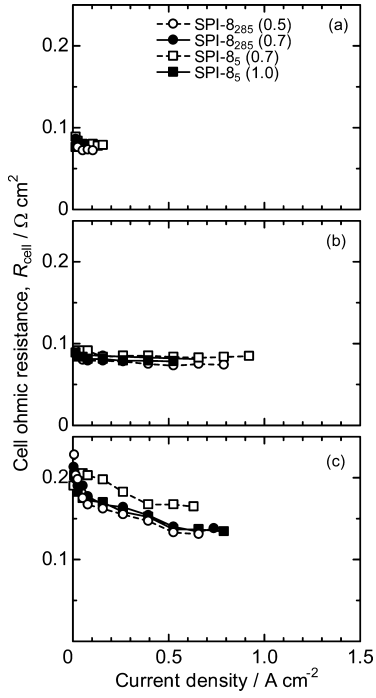

Figure 4. Ohmic resistances of the cells (R_{cell}) for MEAs with SPI-8_{285} (0.5) (open circle), SPI-8_{285} (0.7) (closed circle), SPI-8_5 (0.7) (open square), and SPI-8_5 (1.0) (closed square) binders at (a) 100% RH, (b) 80% RH, and (c) 50% RH at the cell temperature of 80 °C.

proton conduction in the catalyst layer and at the interface between the electrodes and the membrane was sufficient.

At 50% RH, smaller content of SPI-8 binder gave lower cathode performance (Figure 3c). This was more pronounced for the lower molecular weight SPI-8_5. At such low humidity

dx.doi.org/10.1021/am201360j | ACS Appl. Mater. Interfaces 2012, 4, 730−737

where the proton conductivity of SPI-8 (especially SPI-8_5) was low, decrease of binder content caused insufficient proton conducting pathway. In addition, thin cathode layer (due to low content of the binder) tends to dry out because fed gas is more accessible and is more likely to remove the generated water, which further increases its proton conduction resistance. The ohmic resistance of the cell supported the discussion. The MEA with lower content of SPI-8_5 showed the highest ohmic resistance (Figure 4c). As discussed above, the thin cathode layer with low water absorbable SPI-8_5 binder is less likely to provide the generated water to the membrane and to dry the membrane.

To investigate the differences in the properties of MEAs, cyclic voltammograms (CVs) were measured at 40 °C and 100% RH. Figure 5 shows the effect of molecular weight of SPI-8 binder on the CV curves. Hydrogen adsorption/desorption and platinum oxidation/reduction currents increased as the molecular weight of SPI-8 was increased. The ECA values calculated from the hydrogen adsorption charge were 33.4 (SPI-8_5), 39.1 (SPI-8_{50}), and 42.7 (SPI-8_{285}) m^2/g_{-Pt}, respectively. Since proton conductivity at 100% RH was nearly independent of the molecular weight (Figure. S2, Supporting Information), it is considered that the state of the SPI-8 binder covering on the Pt catalysts was different among the ionomers. High molecular weight SPI-8 has better film forming capability and, thus, can have better interfacial contact with the catalysts; i.e., proton conducting channels formed in the ionomer could contact more Pt atoms in the cathode. When Nafion was used as the binder, ECA was 47.8 m^2/g_{-Pt} and slightly higher than that with SPI-8 binders. Since the proton conductivities of SPI-8 and Nafion membranes were comparable at 100% RH (Figure S2, Supporting Information), the differences would reflect the covering states of the binders on Pt/C catalyst. Figure 6 shows the effect of SPI-8 content on the CV curves. For both high molecular weight SPI-8_{285} and low molecular weight SPI-8_5, higher binder content resulted in higher ECA value (Figure 7). These results are in good accordance with the above IV performance in Figures 1c and 3c, where high molecular and/or high content of SPI-8 binder resulted in higher potential. The higher ECAs, i.e., better proton conducting pathway, also played an important role to achieve higher performance at low humidity where proton transport is more crucial.

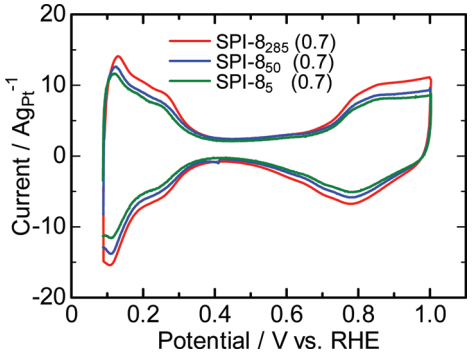

Figure 5. Cyclic voltammograms of CCMs with SPI-8_{285} (red line), SPI-8_{50} (blue line), and SPI-8_5 (green line) binders in fully humidified N_2 at 40 °C. Binder/C ratio was fixed at 0.7.

Humidity Dependence of the Cathode Performance. In order to investigate the effect of humidity on the cathode performance in more detail, mass activities of Pt catalyst, Tafel slopes, and current densities at 0.70 V (IR-free) are plotted as a function of RH in Figure 8. The mass activity (MA) is defined as the current at 0.85 V (IR-free) per unit mass of Pt (A/g_{-Pt}) and is a measure of the catalyst utilization. The MA showed the maximum at medium humidity (70−80% RH) for all electrodes. The low MA at high humidity is ascribed to the insufficient mass transport of oxygen. At low humidity below 80% RH, high molecular and high content of SPI-8 binder resulted in higher MA. As discussed above, this is partly attributable to the improved proton conduction.

In addition, we have investigated the changes in the CV curves at different humidities (Figure 9). We have previously reported that Pt oxidation/reduction charge decreased considerably as the humidity for the gas diffusion electrodes with sulfonated poly(arylene ether) (SPE) binders decreased while the ECA values were rather immune at the same range of humidity.[21,22] The decrease in Pt oxidation/reduction charge was indicative of specific adsorption of the SPE binders onto surface of Pt catalysts to be accountable for the lowered MA values. Similar behavior was observed for the SPI-8 binder. The CV curves and hydrogen adsorption/desorption charges at 70−400 mV vs RHE were nearly identical at 50−100% RH. The results indicate that the proton-conducting pathway in the cathode catalyst layer was properly formed and unaffected by the humidity. In contrast, the CV curves changed at potential region of 650−1000 mV vs RHE with a significant drop of platinum oxidation/reduction charges as the humidity decreases. Figure 10 compares ECA and $Q_{Pt\ oxide}$ of MEAs

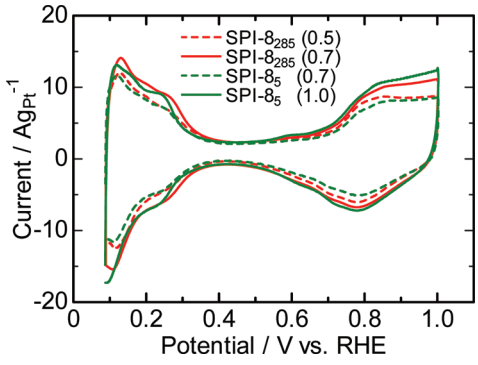

Figure 6. Cyclic voltammograms of CCMs with SPI-8_{285} and SPI-8_5 in fully humidified N_2 at 40 °C. Binder/C ratio was changed from 0.5 (dashed red line) to 0.7 (solid red line) for CCM with SPI-8_{285} and from 0.7 (dashed green line) to 1.0 (solid green line) for CCM with SPI-8_5, respectively.

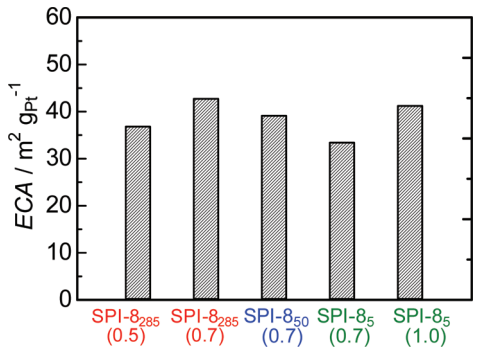

Figure 7. Electrochemically active surface areas (ECAs) of CCMs with SPI-8 binders.

dx.doi.org/10.1021/am201360j | ACS Appl. Mater. Interfaces 2012, 4, 730−737

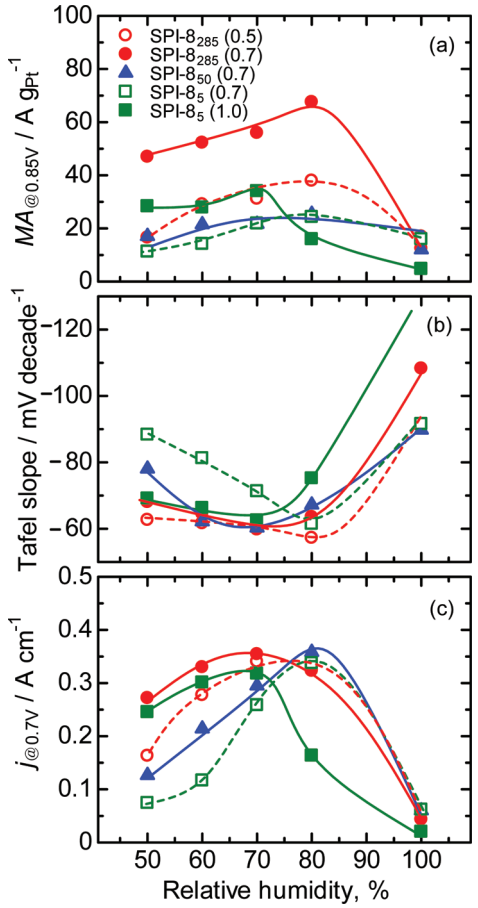

Figure 8. Humidity dependence of (a) mass activity at 0.85 V (MA), (b) Tafel slope, and (c) current density at 0.70 V ($j_{@0.70\,V}$) at T_{cell} = 80 °C.

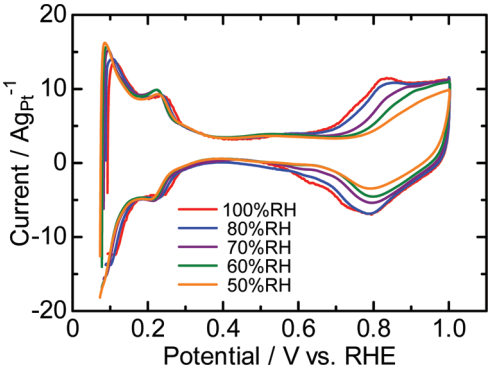

Figure 9. Cyclic voltammograms of CCMs with SPI-8_{50} binders in N_2 at 80 °C and 100% (red line), 80% (blue line), 70% (purple line), 60% (green line), and 50% RH (orange line).

with SPI-8 of different molecular weight and Nafion as a function of RH. Compared with $Q_{Pt\ oxide}$ of Nafion MEA, $Q_{Pt\ oxide}$ of SPI-8 MEA decreased more significantly at lower humidity than 80% RH. It is therefore considered that the specific adsorbability of SPI-8 binder is another factor to cause lower MA values at lower RH. Since a decrease of $Q_{Pt\ oxide}$ was less for SPI-8 binder than for SPE binder, the specific adsorbability of SPI-8 was assumed to be less significant.

The Tafel slopes were calculated from the IR-free polarization curves at low current density, where the effect of oxygen transport was negligibly small. At 70–80% RH, the Tafel slopes

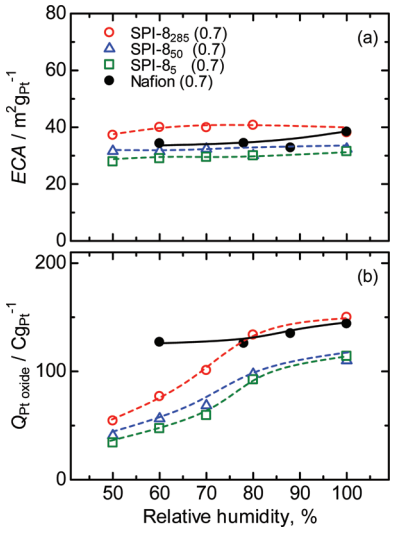

Figure 10. Humidity dependence of electrochemical active surface area (ECA) and Pt oxidation charge ($Q_{Pt\ oxide}$) at 80 °C.

showed minimum values (ca. 60–70 mV/decade), which was close to the theoretical value for kinetically controlled oxygen reduction reaction at 80 °C and implied that both protons and oxygen gases were sufficiently supplied to the Pt catalysts. When the humidity was higher or lower, the balance of oxygen transport and proton conduction was lost, causing higher Tafel slopes.

The current density at 0.70 V (IR-free), $j_{@0.70\ V}$, reflects the overall factors of Pt utilization, proton supply, and the mass transport of oxygen and is often regarded as a measure of total cell performance for automobile and stationary applications. Although the maximum values of $j_{@0.70\ V}$ for all MEAs were ca. 0.35 A/cm^2 at medium humidity (70–80% RH), the appropriate operating conditions were different depending on the composition of MEAs. For instance, the highest $j_{@0.70\ V}$ (= 0.34 A/cm^2) was obtained at SPI-8/C = 0.7 for SPI-8_5 at 80% RH, and the highest $j_{@0.70\ V}$ (= 0.33 A/cm^2) was obtained at SPI-8/C = 1.0 for SPI-8_5 at 70% RH. Unfortunately, there does not seem to exist the best electrode composition for any operating conditions, and instead, each parameter such as proton conductivity, swellability, gas and water permeabilities, specific adsorbability onto the catalysts, and their dependences on humidity needs to be carefully optimized for SPI-8 based CCMs, depending on the operating conditions.

Scanning Transmission Electron Microscopic Observation of SPI-8 Coated Pt/C Catalysts. The morphology of SPI-8 coated Pt/C catalysts at constant binder content of SPI-8/C = 0.7 was observed by scanning transmission electron microscopy (STEM). The bright-field images are shown in Figure 11. The Pt catalysts were clearly observed as black dots of several nanometers in diameter. The layered regions are ascribed to the crystallized carbons. The covering situation of SPI-8 differed with the molecular weight (red dotted lines). The thin layer of SPI-8_{285}, of which thickness was ca. 1–2 nm on average, was not very uniform. There were thinner and thicker areas. SPI-8_{50} seemed to have covered the Pt catalysts somewhat more uniformly compared with SPI-8_{285}. In the case of SPI-8_5 binder, a very thin layer was observed on the surface of the Pt/C catalysts. It is considered that there exist three types of pores, namely, nanopores (<ca. 8 nm in diameter), primary pores (<ca. 40 nm in diameter), and secondary pores

dx.doi.org/10.1021/am201360j | ACS Appl. Mater. Interfaces 2012, 4, 730–737

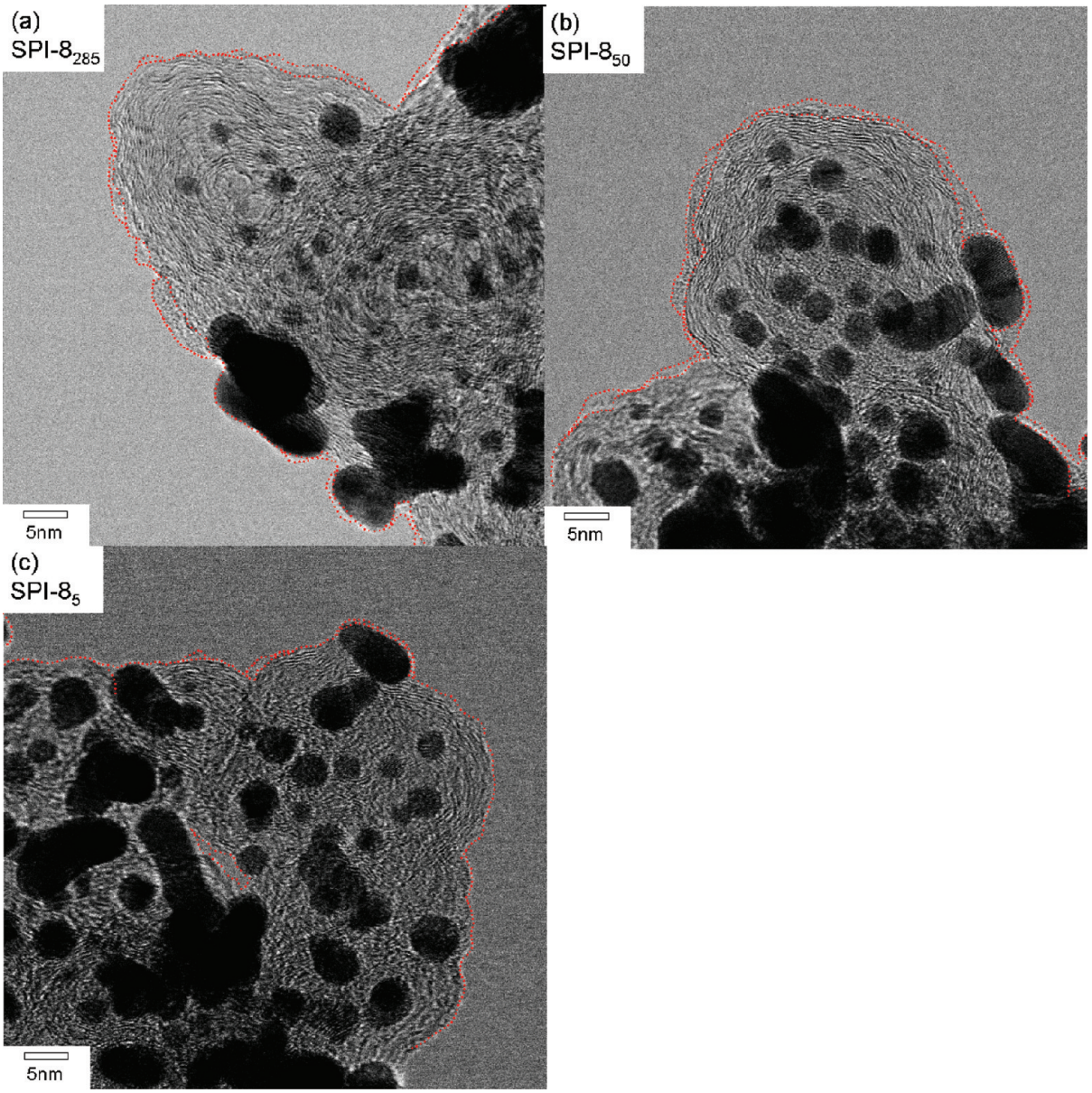

Figure 11. Scanning transmission electron microscopic (STEM) images of Pt/C catalyst coated by (a) SPI-8_{285}, (b) SPI-8_{50}, and (c) SPI-8_5.

(>ca. 40 nm in diameter) in the catalyst layer.[27−29] Primary pores are defined as small pores within agglomerates of carbon particles, and secondary pores are defined as pores among carbon agglomerates. Nanopores are located on the surface of carbon primary particles. In the present case, the differences in the thickness of the binder covering carbon particles may be caused by the differences of the binder situations in nanopores. We then confirmed the presence and situations of nanopores.

The bright-field and dark-field images for SPI-8_5 coated Pt/C catalyst from front-surface (0°) and back-surface (180°) are shown in Figure 12. In the bright-field images, Pt particles that locate on the surface of carbon particles and nanopores can be observed as black dots. In contrary, Pt particles that locate on the surface of carbon particles outside of nanopores are observed as white dots in the dark-field images. Therefore, from the comparison of these images, the presence of Pt catalysts in nanopores could be confirmed. The Pt particles in nanopores are highlighted by yellow dotted lines. A number of small Pt particles located in nanopores were confirmed. It was reported that Nafion as a binder hardly penetrated into nanopores due to its large radii of gyration in polar solutions (several tens of nanometers or larger).[18,28,30,31] Hydrocarbon binders with small radii in solutions are likely to penetrate into nanopores.[18] It is considered that low molecular weight SPI-8 could be the case and accountable for the thin layer of SPI-8_5 binder covering on Pt/C catalysts as observed in Figure 11. In addition, viscosity of binder solutions used for the preparation of catalyst ink might affect the covering states of SPI-8 on the surface of Pt/C catalysts. Dynamic viscosity of 3 wt % SPI-8_{285} in DMSO solution was 89.9 mPas, and those of 3 wt % SPI-8_{50} and 5 wt % SPI-8_5 in DMSO solutions were 28.1 and 10.2 mPas, respectively, at 25 °C. Higher viscosity of SPI-8_{285} solution was likely to cause less uniform coverage of the binder on Pt/C catalysts.

Although it was expected that the formation of proton conducting pathway on Pt particles in nanopores would increase the utilization of Pt catalysts, the ECA and cathode performance were not so improved, as shown in Figures 5 and

dx.doi.org/10.1021/am201360j | ACS Appl. Mater. Interfaces 2012, 4, 730−737

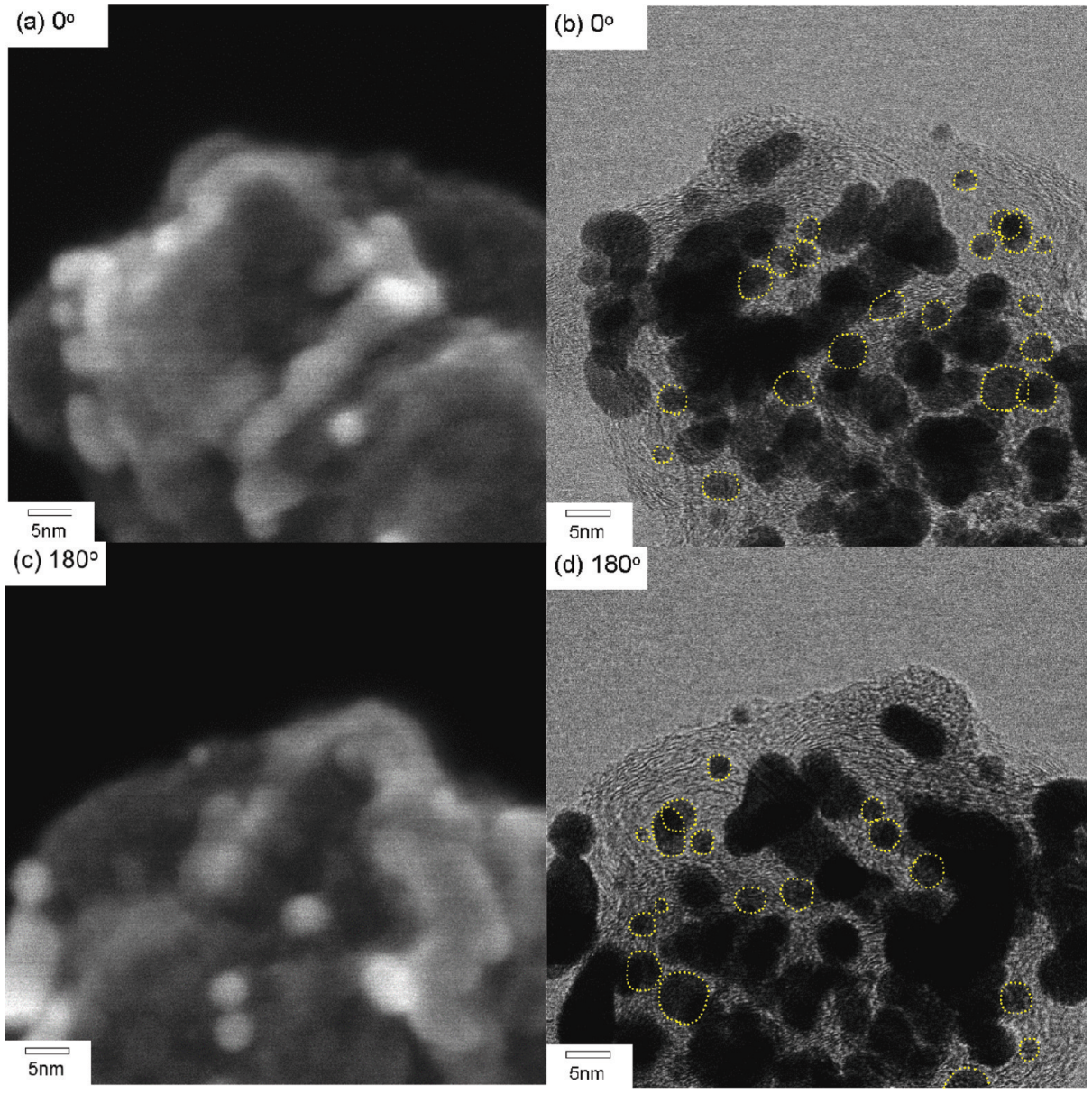

Figure 12. STEM images of SPI-8_5 coated Pt/C catalyst; (a) dark-field image from front-surface (0°), (b) bright-field image from front-surface (0°), (c) dark-field image from back-surface (180°), and (d) bright-field image from back-surface (180°).

8. As discussed above, a number of parameters have to be well-optimized to achieve high cathode performance.[32] Another point that we need to take into account is that ionomers may behave differently in thin layer (nanometer thick) from the membrane in micrometer thick.

CONCLUSION

Sulfonated polyimide (SPI-8) ionomers with different molecular weight were applied as a binder in the catalyst layers, and their fuel cell performances were evaluated at various binder contents and relative humidities. The cathode performance was significantly affected by binder content, molecular weight of the ionomers, and humidity of the supplied gases. The ECAs at 100% RH were improved with increasing content and molecular weight of binders, because high ionomer content provided better proton conducting pathways and higher molecular weight caused better film forming capacity, respectively. With respect to polarization curves under high humidity conditions, larger potential drop at high current density was observed when high molecular weight SPI-8 was used as the binder. Similar results were obtained at higher binder content. These performance losses were due to the insufficient mass transport (oxygen supply and/or water discharge) caused by higher water absorbability in the catalyst layers. Under low humidity conditions, the performances were affected mainly by the proton conductivity of binder rather than the mass transport. While the maximum values of $j_{@0.70\ V}$ were similar for all MEAs, the appropriate operating conditions were different among the electrodes with ionomer composition. Therefore, it is crucial to balance proton conductivity, swellability, gas and water permeabilities, specific adsorbability onto the catalysts, and their dependences on the humidity to achieve superior cathode performance when new ionomer materials will be used as the binder, especially for the cathode.

■ ASSOCIATED CONTENT

Supporting Information

Preparation details of CCMs and water uptake and proton conductivity of SPI-8s. This material is available free of charge via the Internet at http://pubs.acs.org.

■ AUTHOR INFORMATION

Corresponding Author

*K.M.: tel, +81 55 220 8707; e-mail, miyatake@yamanashi.ac.jp. M.W.: tel, +81 55 254 7091; e-mail, m-watanabe@yamanashi.ac.jp.

■ ACKNOWLEDGMENTS

This work was partly supported by the New Energy and Industrial Technology Development Organization (NEDO) through the HiPer-FC Project and the Ministry of Education, Culture, Sports, Science and Technology (MEXT) Japan through a Grant-in-Aid for Scientific Research (23350089 and 23656427).

■ REFERENCES

(1) Rikukawa, M.; Sanui, K. *Prog. Polym. Sci.* **2000**, *25*, 1463−1502.
(2) Jones, D. J.; Roziere, J. *J. Membr. Sci.* **2001**, *185*, 41−58.
(3) Wang, F.; Hickner, M.; Kim, Y. S.; Zawodzinski, T. A.; McGrath, J. E. *J. Membr. Sci.* **2002**, *197*, 231−242.
(4) Hickner, M. A.; Ghassemi, H.; Kim, Y. S.; Einsla, B. R.; McGrath, J. E. *Chem. Rev.* **2004**, *104*, 4587−4611.
(5) Fujimoto, C. H.; Hickner, M. A.; Cornelius, C. J.; Loy, D. A. *Macromolecules* **2005**, *38*, 5010−5016.
(6) Asano, N.; Aoki, M.; Suzuki, S.; Miyatake, K.; Uchida, H.; Watanabe, M. *J. Am. Chem. Soc.* **2006**, *128*, 1762−1769.
(7) Yin, Y.; Suto, Y.; Sakabe, T.; Chen, S. W.; Hayashi, S.; Mishima, T.; Yamada, O.; Tanaka, K.; Kita, H.; Okamoto, K. *Macromolecules* **2006**, *39*, 1189−1198.
(8) Saito, J.; Miyatake, K.; Watanabe, M. *Macromolecules* **2008**, *41*, 2415−2420.
(9) Bae, B.; Miyatake, K.; Watanabe, M. *ACS Appl. Mater. Interfaces* **2009**, *1*, 1279−1286.
(10) Schonberger, F.; Kerres, J.; Dilger, H.; Roduner, E. *Phys. Chem. Chem. Phys.* **2009**, *11*, 5782−5795.
(11) Bae, B.; Hoshi, T.; Miyatake, K.; Watanabe, M. *Macromolecules* **2011**, *44*, 3884−3892.
(12) Easton, E. B.; Astill, T. D.; Holdcroft, S. *J. Electrochem. Soc.* **2005**, *152*, A752−A758.
(13) Higuchi, E.; Okamoto, K.; Miyatake, K.; Uchida, H.; Watanabe, M. *Res. Chem. Intermed.* **2006**, *32*, 533−542.
(14) Kraemer, S.; Puchner, M.; Jannasch, P.; Lundblad, A.; Lindbergh, G. *J. Electrochem. Soc.* **2006**, *153*, A2077−A2084.
(15) Beleke, A. B.; Miyatake, K.; Uchida, H.; Watanabe, M. *Electrochim. Acta* **2007**, *53*, 1972−1978.
(16) Park, J.-S.; Krishnan, P.; Park, S.-H.; Park, G.-G.; Yang, T.-H.; Lee, W.-Y.; Kim, C.-S. *J. Power Sources* **2008**, *178*, 642−650.
(17) Sambandam, S.; Ramani, V. *Electrochim. Acta* **2008**, *53*, 6328−6336.
(18) Lee, C. H.; Lee, S. Y.; Lee, Y. M.; McGrath, J. E. *Langmuir* **2009**, *25*, 8217−8225.
(19) Muldoon, J.; Lin, J.; Wycisk, R.; Takeuchi, N.; Hamaguchi, H.; Saito, T.; Hase, K.; Stewart, F. F.; Pintauro, P. N. *Fuel Cells* **2009**, *9*, 518−521.
(20) Sung, K. A.; Kim, W. K.; Oh, K. H.; Park, J. K. *Electrochim. Acta* **2009**, *54*, 3446−3452.
(21) Yoda, T.; Shimura, T.; Bae, B.; Miyatake, K.; Uchida, M.; Uchida, H.; Watanabe, M. *Electrochim. Acta* **2009**, *54*, 4328−4333.
(22) Yoda, T.; Shimura, T.; Bae, B.; Miyatake, K.; Uchida, M.; Uchida, H.; Watanabe, M. *Electrochim. Acta* **2010**, *55*, 3464−3470.
(23) Kabasawa, A.; Saito, J.; Yano, H.; Miyatake, K.; Uchida, H.; Watanabe, M. *Electrochim. Acta* **2009**, *54*, 1076−1082.
(24) Watanabe, M.; Motoo, S. *J. Electroanal. Chem.* **1975**, *60*, 259−266.
(25) Vogel, W. M.; Baris, J. M. *Electrochim. Acta* **1977**, *22*, 1259−1263.
(26) Yaguchi, T.; Konno, M.; Kamino, T.; Watanabe, M. *Ultramicroscopy* **2008**, *108*, 1603−1615.
(27) Watanabe, M.; Tomikawa, M.; Motoo, S. *J. Electroanal. Chem.* **1985**, *195*, 81−93.
(28) Uchida, M.; Fukuoka, Y.; Sugawara, Y.; Eda, N.; Ohta, A. *J. Electrochem. Soc.* **1996**, *143*, 2245−2252.
(29) Song, J. M.; Suzuki, S.; Uchida, H.; Watanabe, M. *Langmuir* **2006**, *22*, 6422−6428.
(30) Szajdzinskapietek, E.; Schlick, S.; Plonka, A. *Langmuir* **1994**, *10*, 2188−2196.
(31) Wang, S. L.; Sun, G. Q.; Wu, Z. M.; Xin, Q. *J. Power Sources* **2007**, *165*, 128−133.
(32) Lee, M.; Uchida, M.; Yano, H.; Tryk, D. A.; Uchida, H.; Watanabe, M. *Electrochim. Acta* **2010**, *55*, 8504−8512.